Catalysis Today 157 (2010) 397–403

Contents lists available at ScienceDirect

Catalysis Today

journal homepage: www.elsevier.com/locate/cattod

CO_2 reforming of CH_4 over Ni-containing phyllosilicates as catalyst precursors

M.V. Sivaiah[a,b], S. Petit[b], J. Barrault[a], C. Batiot-Dupeyrat[a], S. Valange[a,*]

[a] Laboratoire de Catalyse en Chimie Organique, CNRS UMR 6503 – Université de Poitiers, ESIP, 40 Av. Recteur Pineau, F-86022 Poitiers Cedex, France
[b] HydrASA, UMR CNRS 6269, Université de Poitiers, Bâtiment de Sciences Naturelles, 40 Av. Recteur Pineau, F-86022 Poitiers Cedex, France

ARTICLE INFO

Article history:
Available online 15 June 2010

Keywords:
Nickel
Phyllosilicates
CO_2 reforming
CH_4
Thermal stability

ABSTRACT

CO_2 reforming of CH_4 to synthesis gas was investigated on new grounds using Ni-containing phyllosilicates (PS) as catalyst precursors. Ni-containing 1:1 PS and 2:1 PS were synthesized hydrothermally from a gel containing sodium silicate and nickel chloride, then they were reduced under H_2 flow before being used as catalysts. Several complementary techniques including XRD, TG-DTA, FTIR, and TPR were used to evaluate the structural, thermal, spectroscopic and redox properties of the samples, respectively. Ni 2:1 PS were found to be more thermally stable and catalytically active than Ni 1:1 PS. Well crystallized Ni 1:1 PS thermally treated at 700 °C resulted in a transitional 2:1 PS phase. The reduction of structural nickel in thermally stable PS led to the formation of nanometric Ni^0 particles over the surface of the remaining unreduced PS as well as on silica. The unreduced PS structure with surface OH groups appeared as one of the best supports for Ni^0 nanoparticles, resulting in less coke formation, and thereby leading to a high catalytic stability.

1. Introduction

The production of synthesis gas ($CO + H_2$) through CO_2 reforming of CH_4 (CDRM) over Ni-based catalysts has received considerable attention during the last two decades [1–3]. This process is environmentally of interest because it allows one to convert two undesirable greenhouse gases into a valuable synthesis gas with a H_2/CO ratio of 1, which is more suitable for feeding a Fischer–Tropsch process [1–3]. The CDRM has been investigated over both, noble metals [2–7] and Ni-based [2,3,8–13] supported catalysts. Inherent availability and low cost of nickel when compared to noble metals favor the scaling up of CO_2 reforming reaction. However, the main drawback of the CH_4–CO_2 reforming reaction is the large thermodynamic potential for coke formation, which causes the catalyst deactivation and reactor plugging. Nevertheless it has been reported that a high dispersion of nickel particles over basic supports, as well as a strong interaction between the metal and the support can reduce or suppress the carbon formation [14–18].

In order to control the metal–support interaction, several novel preparation routes or modified known techniques have been investigated, especially for silica supported Ni catalysts [17–19]. Che et al. [17] reported a two-step procedure for the preparation of a Ni/SiO_2 catalyst exhibiting enhanced interaction between Ni and SiO_2. Several authors mentioned that the reaction occurring between Ni species and SiO_2 during the preparation of the catalysts led to the formation of phyllosilicate (PS) phases [17,19]. For example, the silica supported nickel material prepared by deposition–precipitation and ion exchange methods showed considerable amount of 1:1 PS and 2:1 PS phases, respectively [19,20]. Recently, poorly crystallized Ni-containing smectite (a clay mineral similar to 2:1 PS) was prepared and evaluated for CDRM [21]. However, it was found that the catalysts deactivated very quickly due to carbon deposition [21].

To the best of our knowledge, synthetic Ni-containing phyllosilicates have not been explored yet as catalysts precursors for the CO_2 reforming of methane. Ni-containing 2:1 phyllosilicate (Ni 2:1 PS) has the $Ni_3Si_4O_{10}(OH)_2$ structural formula (≈36% of Ni), whereas Ni-containing 1:1 phyllosilicate (Ni 1:1 PS) has the $Ni_3Si_2O_5(OH)_4$ one (≈46% of Ni). The idealized structures of both 1:1 and 2:1 PS are shown in Fig. 1. In Ni 1:1 PS, each layer consists of one tetrahedral sheet (Si coordinated to four oxygen atoms) and one octahedral sheet (Ni coordinated to six oxygen atoms or hydroxyl groups). In the case of a 2:1 PS layer structure, one octahedral sheet sandwiched between two tetrahedral sheets. The detailed description of these structures can be found elsewhere [22–24].

In the present study, Ni 1:1 PS and Ni 2:1 PS were synthesized hydrothermally with variable crystallinity depending on the hydrothermal treatment temperature. Several techniques were used to evaluate their structural (XRD), thermal (TG-DTA), spectroscopic (FTIR) and redox (TPR) properties. All synthesized samples were reduced in situ under a H_2 flow in order to yield the Ni^0 supported catalysts, before being evaluated in the CO_2 reforming of CH_4. Finally, the thermal stability of

* Corresponding author. Tel.: +33 5 49 45 40 48; fax: +33 5 49 45 33 49.
E-mail address: sabine.valange@univ-poitiers.fr (S. Valange).

0920-5861/$ – see front matter © 2010 Elsevier B.V. All rights reserved.
doi:10.1016/j.cattod.2010.04.042

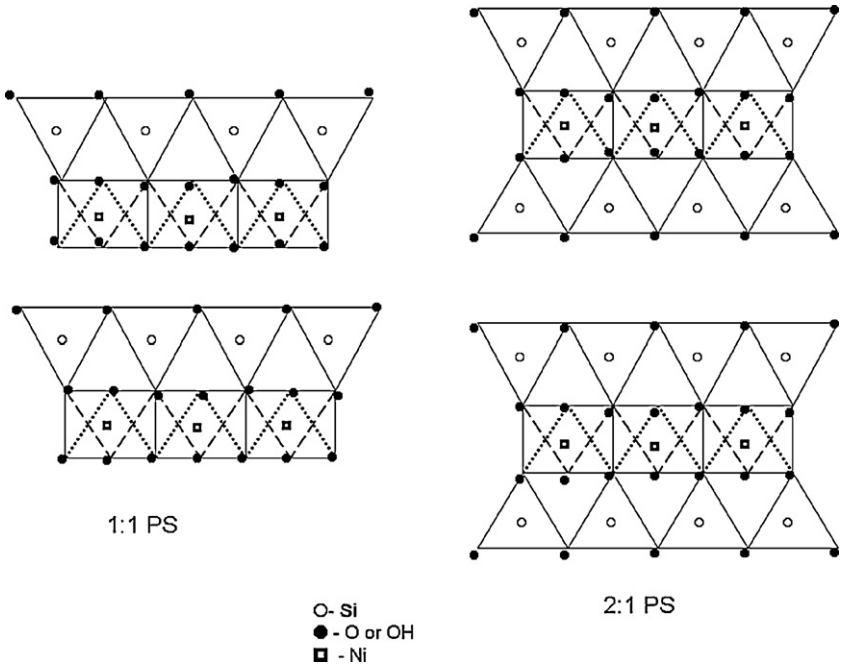

Fig. 1. Idealized structure of 1:1 PS and 2:1 PS.

Ni-based PS was highlighted with regard to their catalytic properties.

2. Experimental

2.1. Synthesis

The hydrothermal synthesis procedure reported by Decarreau [25,26] was adapted to prepare the Ni 1:1 PS and Ni 2:1 PS from a gel containing sodium silicate and nickel chloride. After being hydrothermally treated at 80 and 200 °C, the solid products were separated from the solution by centrifugation and washed repeatedly with distilled water, till the elimination of chloride ions. Then, the Ni-based phyllosilicates were dried in a commercial microwave oven for about 30 min at 85–90 °C (temperature measured with a Raytek laser pyrometer) and thoroughly grinded in an agate mortar before use. The Ni-containing phyllosilicates are labeled L-x and T-x, where L and T refer to the Lizardite (Ni 1:1 PS) and Talc (Ni 2:1 PS) structures and x stands for the experimental synthesis conditions (hydrothermal temperature and duration time). The detailed composition, labels and experimental conditions of the Ni-containing phyllosilicates are shown in Table 1.

2.2. Characterization

Powder wide-angle XRD patterns were recorded on a Panalytical X'pert Pro diffractometer equipped with Cu Kα radiation and operating at 40 kV, 40 mA. Fourier Transformed Infrared spectra were obtained with a Nicolet 510 FTIR spectrometer in the 4000–250 cm^{-1} range. After keeping the KBr pellets (containing 1–2 wt.% of sample) at 110 °C overnight, the spectra were recorded at room temperature (RT) with 4 cm^{-1} resolution in transmission mode. The thermogravimetric analysis of the samples was carried out on a Q600 DTA microbalance from 25 to 1000 °C at a heating rate of 10 °C min^{-1} under an air flow of 100 mL min^{-1}. H_2-TPR experiments were performed on a Micromeritics Autochem 2910 apparatus. The samples (100 mg) were pre-treated in argon at 500 °C for 1 h prior to heating under H_2 flow (5% H_2 + 95% Ar) from 20 to 1000 °C at a heating rate of 5 °C min^{-1}.

2.3. Catalytic test

The CO_2 reforming reaction was carried out in a fixed-bed continuous flow reactor at atmospheric pressure. A weighed amount of catalyst (equivalent to 10 mg of Ni) was mixed with SiC, thoroughly grinded and placed in the reactor. The total quantity of catalyst and SiC was kept constant as 360 mg for all samples. The catalyst was activated with pure H_2 (flow of 35 mL min^{-1}) at 700 °C for 1 h and then cooled down to RT, before the reaction started by introducing a mixture of CH_4 and CO_2 (50:50) with a total flow rate of 100 mL min^{-1} (GHSV = 6×10^5 mL h^{-1} $g_{Ni}{}^{-1}$). The temperature was increased from RT to 700 °C at a heating rate of 10 °C min^{-1} and maintained at this temperature for the desired reaction time. The reaction products were analyzed by online gas phase chromatographs with TCD and FID.

2.4. Data evaluation

The conversion of CH_4 and CO_2, H_2/CO mole ratio, C balance and H_2 balance were followed by the equations:

Conversion of CH_4

$$X_{CH_4} = \frac{F_{in}N^{in}_{CH_4} - F_{out}N^{out}_{CH_4}}{F_{in}N^{in}_{CH_4}} \times 100\ (\%) \quad (1)$$

Conversion of CO_2

$$X_{CO_2} = \frac{F_{in}N^{in}_{CO_2} - F_{out}N^{out}_{CO_2}}{F_{in}N^{in}_{CO_2}} \times 100\ (\%) \quad (2)$$

H_2/CO ratio

$$R_{H_2/CO} = \frac{N^{out}_{H_2}}{N^{out}_{CO}} \quad (3)$$

The determination of the carbon balance allowed us to check that a possible carbon deposit occurred during the catalytic reaction. The carbon balance was determined from the total amount of the products analyzed at the end of the catalytic reaction, divided by

Table 1
Experimental synthesis conditions and TPR data of Ni 1:1 PS and Ni 2:1 PS.

Sample code	Synthesis conditions			TPR data		
	Phyllosilicate type	Temperature (°C)	Time (days)	Temperature maximum (°C)	H_2 consumed (mmol g^{-1})	Theoretical consumption of H_2 (mmol g^{-1})
L1		80	14	562	7.90	
L2	1:1[a]	200	4	555, 720	7.81	7.89[b]
L3		200	14	558, 752	7.47	
T1		80	14	519,[d] 681	5.81	
T2	2:1[c]	200	4	774	6.31	6.22[e]
T3		200	14	799	6.21	

[a] $2SiO_2Na_2O:3NiCl_2:2NaOH$; pH of synthesis ~9.
[b] Molecular weight of $Ni_3Si_4O_{10}(OH)_2$ = 484.4 g.
[c] $4SiO_2Na_2O:3NiCl_2$: 2HCl; pH of synthesis ~6.
[d] s = shoulder.
[e] Molecular weight of $Ni_3Si_2O_5(OH)_4$ = 380.3 g.

the total amount of methane and carbon dioxide introduced in the reactor (Eq. (4)). Moreover, the amount of carbon deposition on spent catalysts was quantified using thermogravimetric analysis.
C balance

$$\mathrm{Cb} = \frac{F_{\mathrm{out}}\left(N_{\mathrm{CO}}^{\mathrm{out}} + N_{\mathrm{CH_4}}^{\mathrm{out}} + N_{\mathrm{CO_2}}^{\mathrm{out}}\right)}{F_{\mathrm{in}}N_{\mathrm{CH_4}}^{\mathrm{in}} + F_{\mathrm{in}}N_{\mathrm{CO_2}}^{\mathrm{in}}} \times 100\ (\%) \quad (4)$$

The hydrogen balance was calculated according to Eq. (5), corresponding to the ratio of the total amount of hydrogen-containing products analyzed at the end of the reaction by the total amount of methane introduced in the reactor.
H_2 balance

$$\mathrm{H_2b} = \frac{F_{\mathrm{out}}\left(N_{\mathrm{H_2}}^{\mathrm{out}} + 2N_{\mathrm{CH_4}}^{\mathrm{out}}\right)}{2F_{\mathrm{in}}N_{\mathrm{CH_4}}^{\mathrm{in}}} \times 100\ (\%) \quad (5)$$

where F_{in} and F_{out} are the total flow rates of the inlet and outlet gases, respectively, N_i^{in} and N_i^{out} are the molar fraction of 'i' in the inlet and outlet gases, respectively.

3. Results and discussion

3.1. XRD data

The wide-angle XRD patterns of Ni 1:1 and Ni 2:1 PS are shown in Fig. 2. Both Ni-based PS synthesized at 200 °C display the characteristic reflections of their corresponding layered structure (JCPDS file nos. 49-1859 and 22-0711) [26] and no other diffraction lines related to NiO. The d_{001} basal spacing of L2 and T2 samples are, respectively, of 0.74 and 0.98 nm. The fact that the d_{001} basal spacing of T2 sample (0.98 nm) is higher than the value of $3 \times d_{003}$ (≈0.945 nm), is attributed to the small number of stacked layers [24]. Poorly crystallized phases are observed for low temperature synthesized samples (80 °C), which exhibit only some *hk* peaks (biperiodic structure), indicating that the layers are stacked turbostratically (Fig. 2a and d) [26]. XRD patterns of reduced L2 and T2 samples at 700 °C (which are used as catalysts for the reforming reaction) show the characteristic peaks of metallic Ni only (Fig. 2i and j). The peaks at 2θ of 44.5° and 51.8° are due to Ni^0 with cubic face centered structure (JCPDS file no. 87-0712). The presence of the PS structure is no more identified in the XRD patterns of the reduced specimens (Fig. 2i and j).

3.2. FTIR data

IR spectra show the characteristic bands of Ni 1:1 PS (L-type samples) and Ni 2:1 PS (T-type samples), with the stretching OH bands at 3649 and 3627 cm^{-1}, respectively (Fig. 3). These bands are also well observed for L1 and T1 samples (80 °C – 14 days), confirming the PS structure for the samples synthesized at low temperature. The ν Si–O modes are resolved as doublet in Ni 1:1 PS samples (Fig. 3), whereas one single band is observed for crystalline Ni 2:1 PS. According to Balan et al. [27,28], the band at 1079 cm^{-1} of L3 compound (200 °C – 14 days) is related to the symmetric stretching of apical Si–O vibration, whereas the band at 978 cm^{-1} of L3 is related to the two degenerated equatorial stretch-

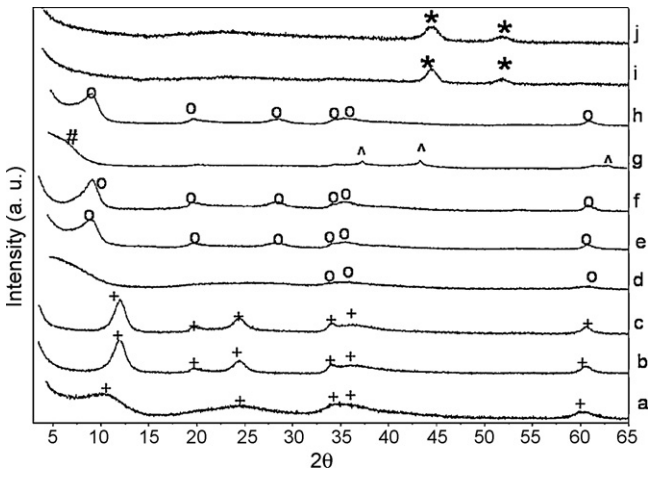

Fig. 2. Powder XRD patterns of Ni 1:1 PS and Ni 2:1 PS (a) L1, (b) L2, (c) L3, (d) T1, (e) T2, (f) T3, (g) L2 calcined at 700 °C, (h) T2 calcined at 700 °C, (i) L2 reduced at 700 °C, and (j) T2 reduced at 700 °C. + = 1:1 PS, o = 2:1 PS, # = Transitional 2:1 PS, ^ = NiO, * = Ni^0.

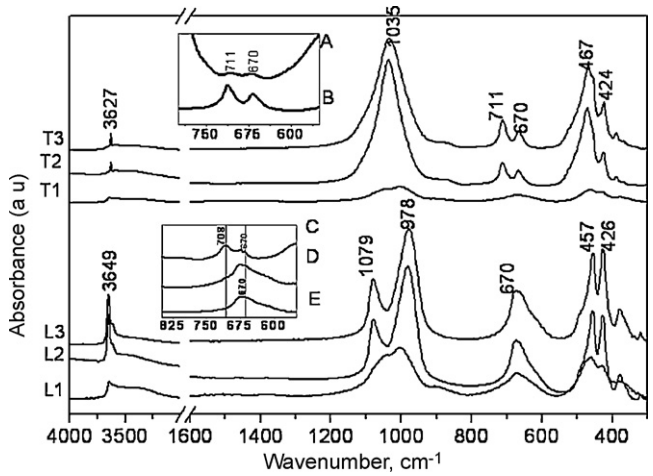

Fig. 3. FTIR spectra of Ni 1:1 PS and Ni 2:1 PS. Inset (A) reduced T2 sample at 700 °C, (B) unreduced T2, (C) untreated L2, (D) L2 thermally treated at 500 °C and (E) L2 thermally treated 700 °C.

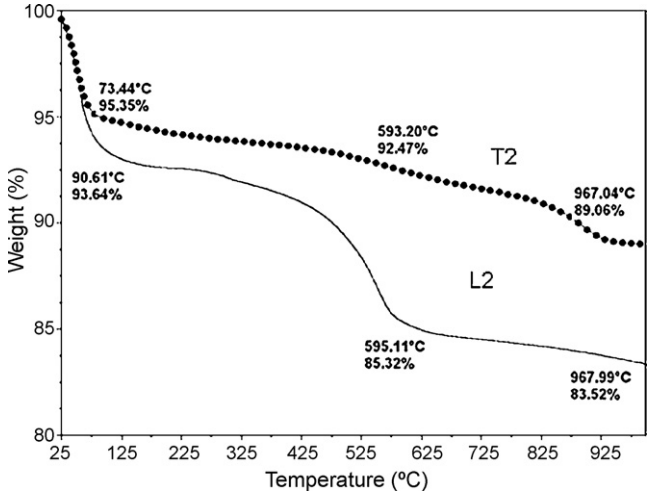

Fig. 4. TG patterns of spent L2 and T2 catalysts (A) and carbon balance during the reaction over reduced L2 and T2 (B). Wt. of sample = 20 mg; Air flow = 100 mL min^{-1}; heating rate = 10 °C min^{-1}.

ing modes (or in-plane vibrations) of Si–O. It has been reported that talc structures (similar to Ni 2:1 PS) exhibit a symmetric peak absorbing around 1020 cm^{-1}, mainly corresponding to the in-plane Si–O vibrations [29,30,20]. In agreement with previously reported results [20], the band centered at 1003 cm^{-1} of L1 sample moves to a lower wavenumber (978 cm^{-1}) for the highly crystalline L3 sample, whereas the band at 1045 cm^{-1} of L1 shifts to higher wavenumber for L3 (1080 cm^{-1}). Well crystallized Ni 2:1 PS samples exhibit a characteristic doublet at 710 and 670 cm^{-1}. These peaks are assigned, respectively, to the δOH vibration and to the tetrahedral Si–O mode vibration in 2:1 layer structure [31]. In the case of Ni 1:1 PS, only one broad band at 670 cm^{-1} integrating the δOH motion is observed. In the case of both PS, the bands observed at ~460 and ~425 cm^{-1} can be assigned mainly to Ni–O–Si vibrations and δSi–O vibrations, respectively [27,28].

FTIR patterns of reduced T2 sample are shown in Fig. S1 (see supporting information). T2 sample (200 °C – 4 days) reduced at 700 °C shows the characteristic δOH bands of 2:1 PS at 711 and 670 cm^{-1}, which indicates the presence of a remaining PS structure. However, when T2 sample is reduced at 900 °C, no peaks related to δOH vibration bands are evidenced, which point out the complete destruction of the 2:1 PS phase. No characteristic bands of OH groups are detected in L2 sample reduced at 700 °C.

3.3. Thermal stability

3.3.1. TGA data

TGA patterns of L2 and T2 samples are shown in Fig. 4. The first weight loss occurring below 150 °C and corresponding to an endothermic peak at about 60–80 °C (not shown) is ascribed to the free absorbed water, whereas the second weight loss observed above 200 °C is due to the removal of structural OH groups. A loss of about 4 and 2.5 structural OH groups is observed for L2 and T2, respectively. Dehydroxylation of L2 sample takes place from 450 to 600 °C (Fig. 4), while that of the corresponding Ni 2:1 PS material (T2 sample) occurs only after 800 °C without any characteristic DTA peak, demonstrating the high thermal stability of the Ni 2:1 PS.

3.3.2. Phase transitions

Powder XRD patterns of both PS after thermal treatment at different temperature (static air atmosphere, heating rate 10 °C min^{-1}, 1 h) illustrate that Ni 2:1 PS are more stable than their Ni 1:1 PS counterparts (Fig. S2), which is in accordance with dehydroxylation of PS observed in TG analysis (Fig. 4). After the thermal treatment at 500 °C, the L1 sample (80 °C – 14 days) is transformed mainly into amorphous silica and Face Cubic Centered (FCC) NiO, whose crystalline nature increases with increasing treatment temperature. At 700 °C, the Ni 1:1 PS synthesized at 200 °C (L2 sample) is transformed into an unidentified transitional phase (broad peak at 1.42 nm) and crystalline NiO (FCC). This behavior is better observed for the well crystallized L3 sample (Fig. S3). FTIR patterns of thermally treated L2 sample at 500 °C, evidenced a broad δOH band around 670 cm^{-1}, which transformed into a doublet in the range of 710 and 670 cm^{-1} (characteristic of a 2:1 PS phase) at 700 °C (Fig. 3 inset C–E). Therefore heat treatment of Ni 1:1 PS at 700 °C (L2 sample) results in a transitional 2:1 PS phase (Tran-2:1 PS). It was already reported that Ni rich 1:1 garnierite (similar to 1:1 PS) with a 0.7 nm d_{001} spacing exhibited a well defined peak around 1.3–1.2 nm after a thermal treatment and that low angle reflection was tentatively ascribed to a Ni-containing sepiolite-like phase (similar to 2:1 PS) [32].

The T2 layered structure (Ni 2:1 PS synthesized at 200 °C for 4 days) is found to be stable up to 700 °C and partial appearance of d_{001} peak even after treating the sample at 900 °C confirms the thermal stability of 2:1 PS phase. Neither Ni-olivine (Ni_2SiO_4) nor Ni-enstatite ($NiSiO_3$) is formed after thermal treatment of Ni 1:1 PS and Ni 2:1 PS at 900 °C, suggesting that NiO can react with SiO_2 only at higher temperature (above 1400 °C), due to anion arrangement constraints [32,33].

3.4. TPR data

TPR patterns (Fig. 5) clearly reveal the absence of $Ni(OH)_2$ or NiO phases in the well crystallized samples (absence of reduction peak below 400 °C). TPR pattern of L3 sample (Ni 1:1 PS synthesized at 200 °C for 14 days) shows a resolved doublet peak (at temperature maxima of 558 and 752 °C), when compared with L1 sample (80 °C – 14 days). In contrast, both Ni 2:1 PS samples synthesized at 200 °C (T2 and T3) exhibit one single and well defined reduction peak at 800 °C. Due to their low thermal stability, the reduction of Ni present in 1:1 PS occurs at a lower temperature than their 2:1 counterparts. The doublet TPR pattern of L2 and L3 compounds can be attributed to their thermally transformed Tran-2:1 PS phase.

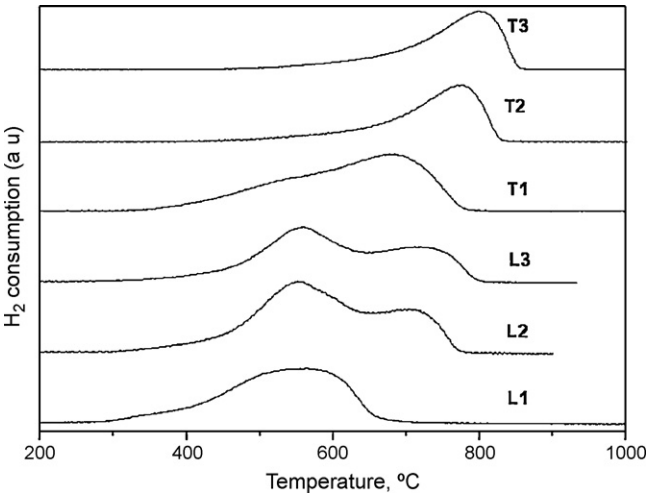

Fig. 5. TPR patterns of Ni 1:1 PS and Ni 2:1 PS. Wt. of sample = 100 mg, 5% H_2 + 95% Ar; flow = 50 mL min^{-1}; heating rate = 5 °C min^{-1}. *Note*: All samples are preheated to 500 °C under Ar atmosphere. Except for L1 sample, the structure of all samples is stable even after thermal treatment at 500 °C (Fig. S2. See supporting information).

Table 2
Catalytic activity and stability of Ni 1:1 PS and Ni 2:1 PS.

Catalyst	Conversion at 12 h of reaction		% Decrease in conversion after 12 h		H_2/CO ratio after 12 h
	CH_4	CO_2	CH_4	CO_2	
L1	16.4	23.7	25.5	24.8	0.8
L2	20.8	30.6	43.5	33.8	0.7
L3	29.0	39.3	12.0	8.5	0.8
T1	37.6	47.7	–	–	0.8
T2	34.0	50.5	4.0	7.0	1.1
T3	39.3	60.7	5.8	14.0	0.7
T2 reduced at 900 °C	16.7	35.2	52.3	29.5	0.7

Conditions: Wt. of Ni = 10 mg, reduction at 700 °C, reaction temperature = 700 °C, CH_4:CO_2 = 50:50, flow = 100 mL min^{-1}.

Reduction of structural Ni in this Tran-2:1 PS needs a higher temperature than that required for Ni in 1:1 PS phase.

The amount of H_2 consumed during the reduction process of both PS is shown in Table 1. It can be noticed from the H_2 consumption for the reduction of L1 and L2 samples that Ni species are reduced almost quantitatively. More than 95% of Ni in L3 sample (Ni 1:1 PS synthesized at 200 °C for 14 days) is reduced. In the case of Ni 2:1 PS, the amount of H_2 consumed during the TPR experiments is in agreement with the amount of Ni in T2 and T3 compounds (synthesized at 200 °C). Whereas for T1 sample (80 °C – 14 days), the gel prepared according to the 2:1 PS composition is slightly acidic (pH ∼ 6) and a part of Ni is observed in the centrifuged fraction (solution phase) (Table 1). Thus, a lower content of Ni in T1 sample results in a lower H_2 consumption during TPR measurement (Table 1). This observation points out that a higher temperature is necessary to prepare the Ni 2:1 PS.

From the TPR results, it can be highlighted that (i) Ni in both PS is nearly totally reduced during the TPR measurement and (ii) the reducibility of Ni slightly decreases with the increase of the crystallinity of PS (Table 1).

3.5. CO_2 reforming of CH_4

3.5.1. CH_4 and CO_2 conversion

The methane reforming reaction was carried out over the reduced Ni 1:1 PS and Ni 2:1 PS samples at atmospheric pressure, using a mixture of CH_4 and CO_2 without any dilution of gases. Both PS are subjected to reduction (as described in Section 2.3) before the reaction. The labels of both PS are used as it is, while describing their catalytic properties. As shown in Fig. 6A and B, the catalytic activity of Ni 2:1 PS compounds is always higher than that of the corresponding Ni 1:1 PS counterparts. Moreover, the increase in crystallinity of both Ni-based PS (L3 and T3 samples) leads to a more important conversion of CO_2 than CH_4. The catalytic conversion of CO_2 and CH_4 after 12 h of reaction, coupled to the catalytic stability value indicate that Ni 2:1 phyllosilicates exhibit a higher catalytic stability than Ni 1:1 PS phases (Table 2). Due to the high thermal stability of Ni 2:1 PS, the Ni in the structure requires a higher temperature (more than 700 °C) to be reduced into Ni^0 than in Ni 1:1 PS phases (Fig. 5). This indicates (i) a partial reduction of Ni in 2:1 PS structure, which results in less Ni^0 metal–metal interaction, thereby in less Ni^0 sintering, and (ii) that the remaining unreduced 2:1 PS acts as support for Ni^0 together with SiO_2.

XRD patterns recorded after reduction at 700 °C of L2 and T2 samples clearly show the presence of metallic nickel in both samples (Fig. 2i and j). The observed differences in the FWHM of the (1 1 1) diffraction lines point out the smaller size of the Ni^0 particles formed after reduction of T2 sample (Fig. 2j) than those of L2 specimen (Fig. 2i). The mean crystal domain size measured by the Scherrer equation of reduced T2 and L2 are, respectively, of 6 and 7.4 nm. TEM characterization performed after TPR experiments (not shown here) indicates that the Ni^0 particles size varies from 4 to 15 nm (average diameter 9 nm) for T2 and from 5 to 24 nm (average diameter 14 nm) for L2 sample. According to previously reported CO_2 reforming results on reduced Ni/SiO_2 catalysts, lower Ni^0 particles size and less metal–metal interactions appear as a prerequisite for high catalytic activity [1,34]. Thus, the higher catalytic activity of Ni 2:1 PS can be due to the partial reduction of Ni and/or the higher thermal stability of these 2:1 PS materials compared with Ni 1:1 PS ones. The higher activity exhibited by L3 when compared with the corresponding low temperature synthesized L1 sample may be explained in a similar way. As mentioned earlier (Section 3.3), the thermal treatment of L3 at 700 °C leads to a Tran-2:1PS phase. It can be noticed from the TPR pattern of L3 sample that only 60% of Ni is reduced up to 700 °C (Fig. 5). Hence, the partial

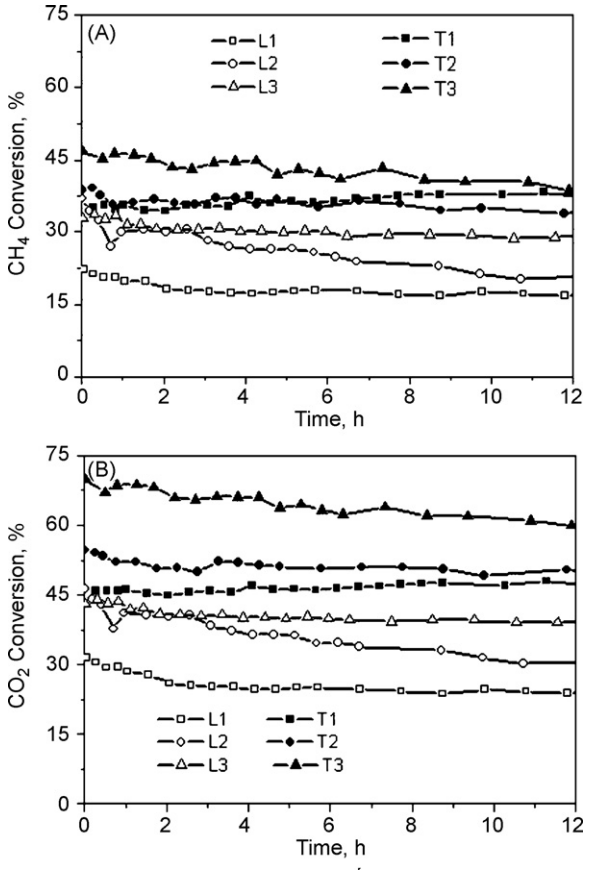

Fig. 6. Conversion of (A) CH_4 and (B) CO_2 over reduced Ni 1:1 PS and Ni 2:1 PS. Wt. of Ni = 10 mg, reduction at 700 °C, Reaction temperature = 700 °C, CH_4:CO_2 = 50:50, flow = 100 mL min^{-1}.

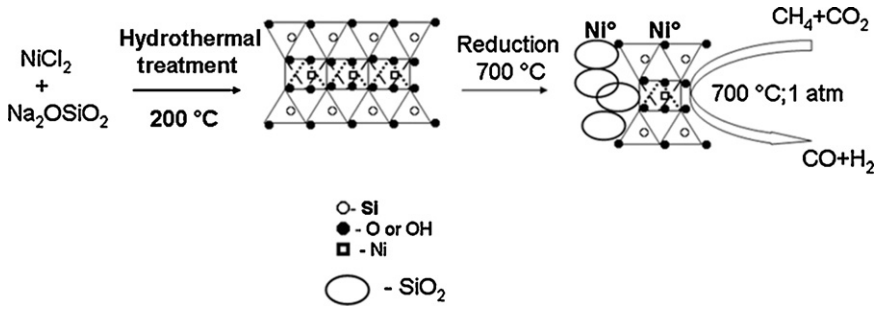

Fig. 7. Schematic representation of Ni 2:1 PS as catalyst precursor for CO_2 reforming reaction.

reduction of Ni in L3 leads to an unreduced PS phase, which acts as a support for Ni^0 particles, thereby increasing the catalytic activity. In the case of L1 sample, the complete reduction of Ni leads to Ni^0 particles supported on SiO_2 only.

XRD patterns of reduced L2 and T2 samples at 700 °C do not show any characteristic peak of a PS structure (Figs. 2i and j and S1). However, the FTIR spectrum of the reduced T2 sample shows the characteristic band of δOH vibrations (Fig. 3, inset A and B), indicating the presence of a remaining PS structure. Various authors have shown that the CH_4 dissociation over a Ni^0/support surface took place via the formation of various CH_x species [34–36]. Bradford and Vannice [1] mentioned that surface hydroxyl (OH) groups can interact with CH_x species, which can further dissociate. It is also interesting to note that a remarkable increase of the CO_2 conversion is observed over well crystallized samples (T3 and L3) oppositely to poorly crystallized samples (T1 and L1). Therefore, our results point out that the presence of structural OH groups, as well as the nature of the support, greatly enhances the CO_2 conversion. A schematic representation of Ni 2:1 PS as catalyst precursor for CO_2 reforming reaction is shown in Fig. 7. The catalytic activity of T2 sample reduced at higher temperature (900 °C instead of 700 °C) shows a drastic decrease in catalytic activity and stability (Table 2 and Fig. S4). The 2:1 PS structure of T2 is completely modified after reduction at 900 °C (Fig. S1). Thus, SiO_2 is the only support for Ni particles. The increase in Ni^0 mean crystal domain size can also account for the lower catalytic properties of T2 sample reduced at 900 °C (Fig. S1). This study also points out that SiO_2 as support for Ni^0 particles and higher Ni^0 particles size cause the poor catalytic activity. In the case of T2 sample reduced at 700 °C, the remaining unreduced PS structure as a part of Ni^0 particles support as well as lower particle sizes of Ni^0 are responsible for the higher catalytic activity (Table 2 and Fig. S1).

3.5.2. H_2/CO ratio

All the catalysts show a higher CO_2 conversion than that of CH_4 (Fig. 6 and Table 2). It can be assumed that CO_2 is consumed simultaneously in the reverse water gas shift reaction (RWGS: $CO_2 + H_2 \rightarrow CO + H_2O$). This assumption is substantiated by the fact that low (less than one) H_2/CO molar ratios are observed during the reaction, except for T2 sample (H_2/CO molar ratio is above 1 even after 12 h of time on stream). Fig. 8 clearly shows the negative H_2 balance during the reaction except for T2 sample. This indicates that the RWGS reaction occurs simultaneously with the reforming reaction. Thus, higher CO_2 conversion than CH_4 conversion is mainly due to the reaction between H_2 and CO_2. The detailed study of the catalytic activity of these Ni-based phyllosilicates towards RWGS will be investigated to elucidate the effect of RWGS in the reforming reaction.

3.5.3. Carbon deposition and catalytic stability

As mentioned in the Section 2, if a carbon balance discrepancy was observed, this means that coke formation occurred during the catalytic reaction. The amount of carbon deposition on spent catalysts was then quantitatively determined by thermogravimetric analysis. As shown in Fig. 9, the TGA results of the spent catalysts are in agreement with those of the carbon balance. Indeed, the amount of carbon deposits after the reforming reaction is, respectively, of ~0.3% and 2.2% for T2 and L2 samples. By taking into account the dilution factor due to SiC, the amount of carbon deposition is found to be ~1% and 22%, respectively. Moreover, after 12 h of reaction over T2 and L2, a decrease in CH_4 conversion, respectively, of 4% and 45% is observed (Table 2). Thus, the absence of coke deposit on

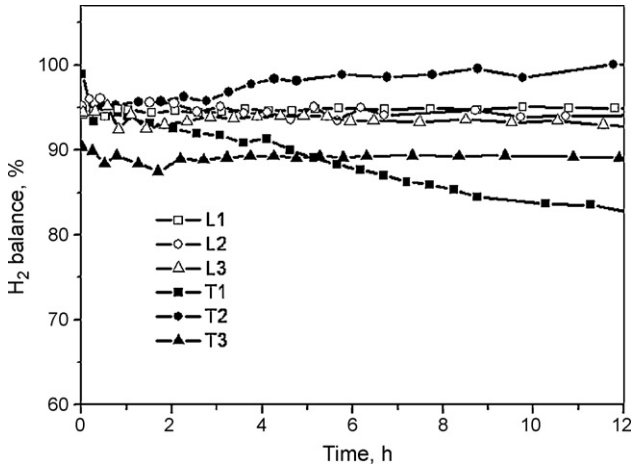

Fig. 8. H_2 balance during the reforming reaction over reduced Ni 1:1 PS and Ni 2:1 PS.

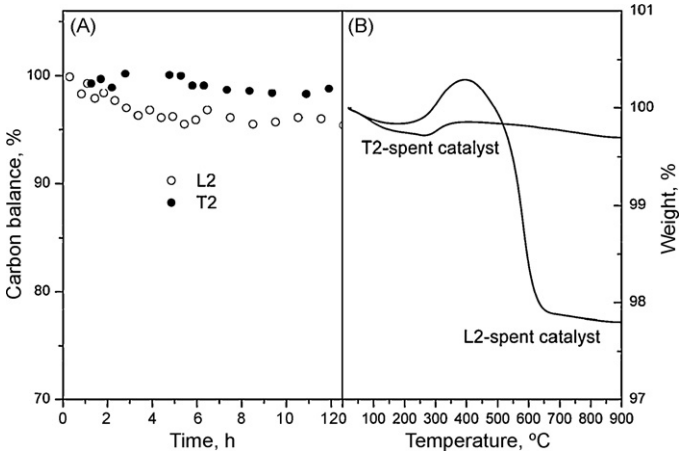

Fig. 9. (A) Carbon balance during the reforming reaction over reduced L2 and T2 catalysts and (B) TG pattern of spent L2 and T2 catalysts. For TGA studies, Wt. of sample (Ni-containing PS + SiC) = ~60 mg; air flow = 100 mL min^{-1}; heating rate = 10 °C min^{-1}.

spent T2 sample results in a far higher catalytic activity and stability of T2 sample than for the corresponding L2 compound.

Leroi et al. [37] studied the carbon formation from acetylene decomposition on antigorite-based Ni^0 (1:1 PS structure). Carbon growth was hardly observed on partially reduced nickel antigorite samples. In fact, carbon formation occurred in areas where unreduced nickel antigorite layered structure did not exist [37]. This implies that Ni^0 supported on unreduced PS structure does not favor the coke formation. Moreover, recent studies have shown that the presence of surface OH groups decreased the possibility of CH_x scission into surface carbon species [38]. In the particular case of T2 sample, the remaining unreduced PS structure (with OH groups) as support for Ni^0 could prevent the coke formation during the reaction. Thus, the present study demonstrates that well crystallized and thermally stable Ni-containing phyllosilicates are efficient catalyst precursors for the CO_2 reforming of CH_4.

4. Conclusion

For the first time, hydrothermally synthesized Ni-containing 1:1 and 2:1 phyllosilicates (PS) are used as catalyst precursors for CO_2 reforming of CH_4. XRD and FTIR investigations on thermally treated Ni 1:1 PS clearly reveal the formation of a transitional phase similar to 2:1 PS. Ni-based 2:1 phyllosilicates materials prove thermally stable and exhibit excellent catalytic properties when compared with Ni 1:1 PS compounds. Partial reduction of Ni species in thermally stable PS phases results in well dispersed nanometric Ni^0 particles. Moreover, the remaining unreduced PS structure with surface OH groups serves as better support for Ni^0 nanoparticles and is shown to inhibit the coke formation, thereby enhancing the catalytic stability. Our results demonstrate that thermally stable Ni-containing PS materials are highly promising catalysts compared with the ones used until now for CO_2 reforming of CH_4.

Acknowledgement

The author (M.V.S.) gratefully acknowledges CNRS and University of Poitiers for the awarding of postdoctoral fellowship.

Appendix A. Supplementary data

Supplementary data associated with this article can be found, in the online version, at doi:10.1016/j.cattod.2010.04.042.

References

[1] M.C.J. Bradford, M.A. Vannice, Catal. Rev.: Sci. Eng. 41 (1999) 1–42.
[2] E. Ruckenstein, Y.H. Hu, Adv. Catal. 48 (2004) 297–345.
[3] S.C. Tsang, J.B. Claridge, M.L.H. Green, Catal. Today 23 (1995) 3–15.
[4] S. Damyanova, B. Pawelec, K. Arishtirova, M.V. Martinez Huerta, J.L.G. Fierro, Appl. Catal. B: Environ. 89 (2009) 149–159.
[5] Z.-J. Wang, Y. Zhao, L. Cui, H. Du, P. Yao, C.-J. Liu, Green Chem. 9 (2007) 554–559.
[6] Z. Hou, P. Chen, H. Fang, X. Zheng, T. Yashima, Int. J. Hydrogen Energy 31 (2006) 555–561.
[7] M. García-Diéguez, I.S. Pieta, M.C. Herrera, M.A. Larrubia, I. Malpartida, L.J. Alemany, Catal. Today 149 (2010) 380–387.
[8] C.E. Daza, J. Gallego, F. Mondragón, S. Moreno, R. Molina, Fuel 89 (2010) 592–603.
[9] G. Valderrama, A. Kiennemann, M.R. Goldwasser, J. Power Sources 195 (2010) 1765–1771.
[10] A.S.A. Al-Fatish, A.A. Ibrahim, A.H. Fakeeha, M.A. Soliman, M.R.H. Siddiqui, A.E. Abasaeed, Appl. Catal. A: Gen. 364 (2009) 150–155.
[11] S. Liu, L. Guan, J. Li, N. Zhao, W. Wei, Y. Sun, Fuel 87 (2008) 2477–2481.
[12] G.S. Gallego, F. Mondragón, J. Barrault, J.-M. Tatibouët, C. Batiot-Dupeyrat, Appl. Catal. A: Gen. 311 (2006) 164–171.
[13] A. Djaidja, S. Libs, A. Kiennemann, A. Barama, Catal. Today 113 (2006) 194–200.
[14] K. Tomishige, Y. Chen, O. Yamazaki, Y. Himeno, Y. Koganezawa, K. Fujjimoto, Stud. Surf. Sci. Catal. 119 (1998) 861–866.
[15] T. Horiuchi, K. Sakuma, T. Fukui, Y. Kubo, T. Osaki, T. Mori, Appl. Catal. A: Gen. 144 (1996) 111–120.
[16] S.B. Wang, G.Q.M. Lu, Energy Fuels 12 (1998) 248–256.
[17] M. Che, Z.X. Cheng, C. Louis, J. Am. Chem. Soc. 117 (1995) 2008–2018.
[18] Y.-X. Pan, C.-J. Liu, P. Shi, J. Power Sources 176 (2008) 46–53.
[19] P. Burattin, M. Che, C. Louis, J. Phys. Chem. B 103 (1999) 6171–6178.
[20] M. Kermarec, J.Y. Carriat, P. Burattin, M. Che, A. Decarreau, J. Phys. Chem. 98 (1994) 12008–12017.
[21] N. Iwasa, M. Takizawa, M. Arai, Appl. Catal. A: Gen. 314 (2006) 32–39.
[22] http://www.tulane.edu/~sanelson/eens211/phyllosilicates.htm.
[23] G.W. Brindley, H.-M. Wan, Am. Mineral. 60 (1975) 863–871.
[24] G.W. Brindley, D.L. Bish, H.-M. Wan, Am. Mineral. 64 (1979) 615–625.
[25] A. Decarreau, Bull. Miner. 103 (1980) 579–590.
[26] H. Mondesir, A. Decarreau, Bull. Miner. 110 (1987) 409–426.
[27] E. Balan, M. Saitta, F. Mauri, C. Lemaire, F. Guyot, Am. Mineral. 87 (2002) 1286–1290.
[28] E. Balan, F. Mauri, C. Lemaire, C. Brouder, F. Guyot, A.M. Saitta, B. Devouard, Phys. Rev. Lett. 89 (2002) 177401–177404.
[29] V.C. Farmer, The Infrared Spectra of Minerals, Mineralogical Society, London, 1974.
[30] S. Yariv, L. Heller-Kallai, Clays Clay Miner. 23 (1975) 145–152.
[31] P. Gerard, A.J. Herbillon, Clays Clay Miner. 31 (1983) 143–151.
[32] P.T. Hang, G.W. Brindley, Clays Clay Miner. 21 (1973) 51–57.
[33] S. Yishinori, M. Kenji, Y. Tsutomu, Int. J. Miner. Process. 19 (1987) 253–261.
[34] V.C.H. Kroll, H.M. Swaan, C. Mirodatos, J. Catal. 161 (1996) 409–422.
[35] T. Osaki, H. Masuda, T. Mori, Catal. Lett. 29 (1994) 33–37.
[36] J. Erkelens, W.J. Wösten, J. Catal. 54 (1978) 143–154.
[37] P. Leroi, F.J.C.S. Aires, T. Goislard de Monsabert, H. Le Poche, J. Dijon, J.L. Rousset, J.C. Bertolini, Appl. Catal. A: Gen. 294 (2005) 131–140.
[38] S.-G. Wang, D.-B. Cao, Y.-W. Li, J. Wang, H. Jiao, Surf. Sci. 603 (2009) 2600–2606.